## Supporting Information

# Changes in the hydration structure of imidazole upon protonation: Neutron scattering and molecular simulations

Elise Duboué-Dijon[1,a)], Philip E. Mason[1,b)], Henry E. Fischer[2)], Pavel Jungwirth[1)]

[1]*Institute of Organic Chemistry and Biochemistry, Czech Academy of Sciences, Flemingovo nam. 2, 16610 Prague 6, Czech Republic*

[2]*Institut Laue-Langevin, 71 avenue des Martyrs, CS 20156, 38042 Grenoble cedex 9, France*

## 1. Neutron scattering patterns

The neutron scattering patterns obtained for each of the 8 samples are shown in FIG. S**1** after correction for multiple scattering and absorption as well as normalization versus a standard vanadium rod. The first obvious difference between the various samples is that the total scattering intensity is larger for light water than for heavy water solutions, which is a consequence of the very high incoherent scattering cross section of the H nucleus. Light water solutions also exhibit a much more pronounced slope in the data, which is due to the stronger inelastic and incoherent scattering, the so-called Placzek effect, of the H nucleus.

[a] Author to whom correspondence should be addressed. Electronic mail: elise.duboue-dijon@uochb.cas.cz
[b] Author to whom correspondence should be addressed. Electronic mail: philip.mason@uochb.cas.cz

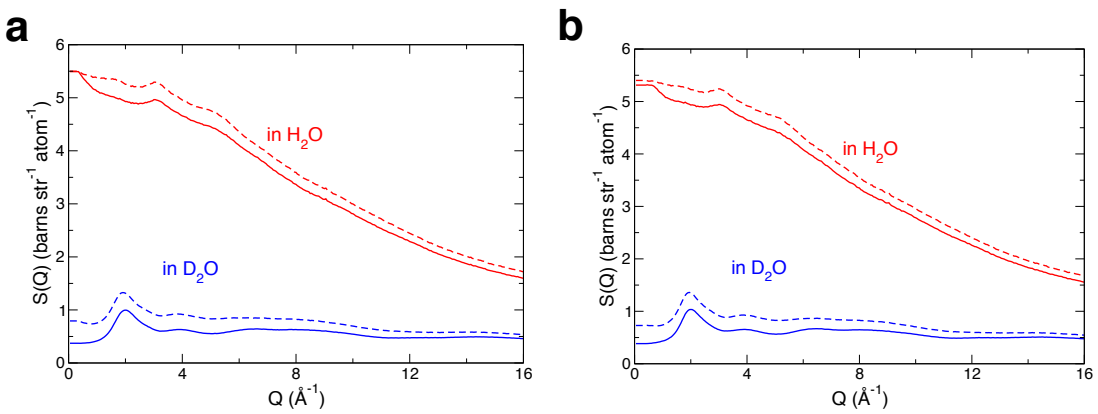


FIG. S1. Total neutron scattering patterns *S(Q)* of a) the 4 3 m imidazole solutions and b) the 4 3 m imidazolium chloride solutions. Solutions in $H_2O$ are plotted in red, while $D_2O$ solutions are shown in blue. Solid lines are employed when the solute non-exchangeable hydrogen atoms are $^1H$, while data for solutions with a deuterated solute are shown in dashes.

## 2. First and second order differences.

For the 3 m imidazolium chloride solutions, the first order differences are expressed, with prefactors in millibarns, as:

$$\begin{aligned} {}^{imidazolium}\Delta S^{D_2O}_{HsubX}(Q) = {} & 36.7\ S_{HsubHex}(Q) + 15.2\ S_{HsubOw}(Q) + 2.64\ S_{HsubN}(Q) \\ & + 2.81\ S_{HsubC}(Q) + 0.62\ S_{HsubHsub}(Q) + 1.35\ S_{HsubCl}(Q) - 59.3 \end{aligned} \quad \text{(S1)}$$

$$\begin{aligned} {}^{imidazolium}\Delta S^{H_2O}_{HsubX}(Q) = {} & -20.6\ S_{HsubHex}(Q) + 15.2\ S_{HsubOw}(Q) + 2.64\ S_{HsubN}(Q) \\ & + 2.81\ S_{HsubC}(Q) + 0.62\ S_{HsubHsub}(Q) + 1.35\ S_{HsubCl}(Q) - 1.99 \end{aligned} \quad \text{(S2)}$$

Direct subtraction of the two first order differences yields the second order difference ${}^{imidazolium}\Delta\Delta S(Q)$. It can be expressed as a function of a single pair-wise structure factor ${}^{imidazolium}S_{HsubHex}(Q)$:

$${}^{imidazolium}\Delta\Delta S\ (Q) = {}^{imidazolium}\Delta S^{D_2O}_{HsubX}(Q) - {}^{imidazolium}\Delta\Delta S^{H_2O}_{HsubX}(Q) = 57.3\ {}^{imidazolium}S_{HsubHex}(Q) - 57.3 \quad \text{(S3)}$$

FIG. S**2** complements FIG. 3 in the main text and shows (blue curves) the difference between the experimental and computed neutron signal.

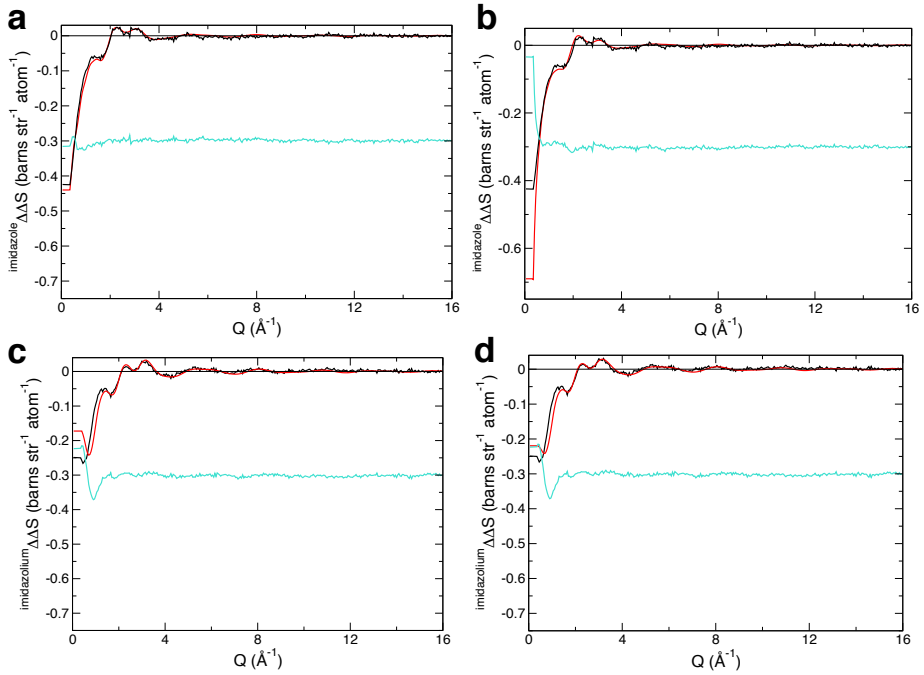


FIG. S2. Same as FIG. 3 in the main text, with the addition in blue on each panel of the difference between the simulation and experimental signal. The difference curves are shifted by -0.3 on the y-axis for clarity purposes.

## 3. Mode of interaction between imidazole molecules

FIG. S3 shows the density maps of imidazole hydrogen, carbon and nitrogen atoms around an imidazole molecule. It clearly shows that one mode of interaction between two imidazole molecules is to form an hydrogen bond between the donor N1 of one molecule and the acceptor N3 of the other. Two imidazole molecules also interact with a weak orientational preference in a "T-shape" mode, a CH group of an imidazole molecule pointing towards the ring of another imidazole molecule. However, one must keep in mind that our classical simulations do not explicitly describe the electronic specificity of the aromatic ring and that the preferred mode of association between imidazole molecules (T-shape vs stacking) could thus not be reliably captured by our MD simulations.

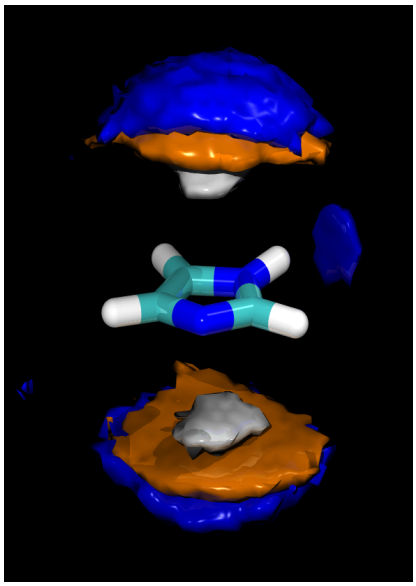

FIG. S3. Density maps of imidazole hydrogen (white), carbon (orange) and nitrogen (blue) atoms around an imidazole solute for a 3 m a imidazole solution described with the CGenFF force field. The density contour levels are drawn for 3.3 times the bulk density of each nuclei.

## 4. Analysis of cluster sizes in the imidazolium chloride solution

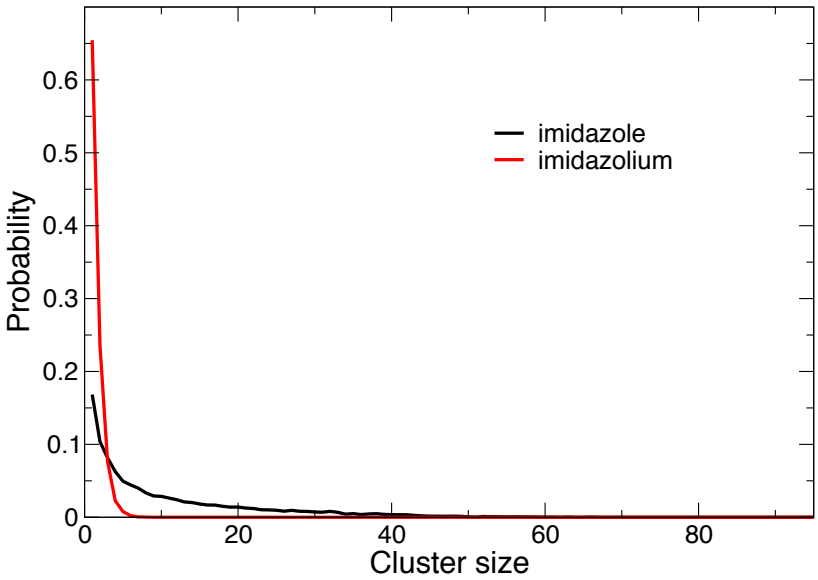


FIG. S4. Probability for an imidazole (black) / imidazolium (red) molecule to be part of a cluster of a given size in a simulation of a 3 m imidazole / imidazolium chloride solution, imidazole being described with the CGenFF force field and imidazolium with the full charges CGenFF force field.

## 5. Influence of the water model

The simulation of the 3 m imidazole solution was repeated with different water models – SPCE (main text), the original TIP3P model and the CHARMM TIPS3P version, with

Lennard-Jones parameters added on the water hydrogens. FIG. S**5** compares the second order differences obtained with the different water models. The differences are very minor which shows that the results presented in this study are rather insensitive to the chosen water model.

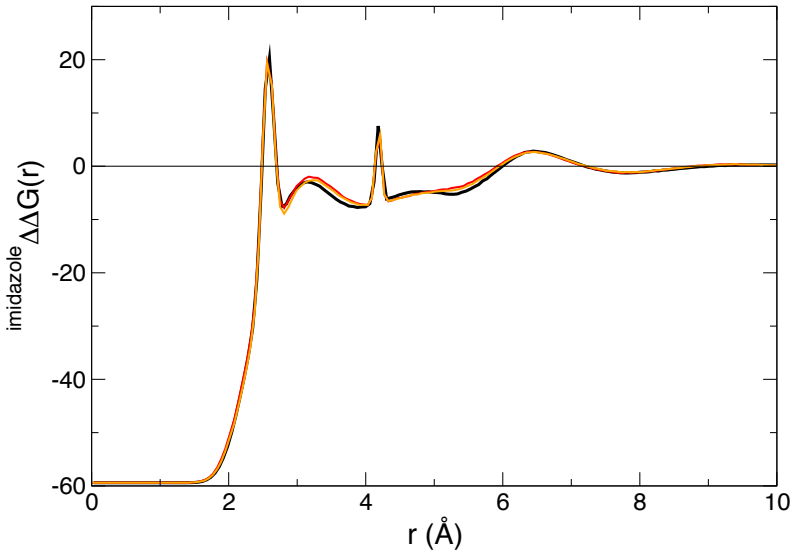


FIG. S5. Second order differences in the r-space *ΔΔG(r)* as obtained from MD simulations of a 3 m imidazole solution using the SPCE (black), the original TIP3P (red) and the CHARMM TIPS3P (orange) water model.

## 6. Fourier transform and post-treatment of Q-space data.

In principle, one can Fourier-transformed the experimental Q-space signal to convert it into an experimental r-space representation. However, despite the excellent counting statistics of the D4C instrument, inevitable counting errors lead to ringing in the Fourier transform of the Q space data. Indeed, FIG. S**6** (black curve) shows that the raw Fourier transform of the experimental signal, without any smoothing of the Q-space data before treatment exhibits significant ringing artifacts. On the other end FIG. S**6** (blue curve) shows the Fourier transform of the experimental data after the application of a hard window function, which terminates the data to zero in the range 5-7 $Å^{-1}$. This treatment is effective at reducing the ringing artifacts, but it comes at the expense of significantly reducing the resolution of the real space data. In red is shown the Fourier transform of the experimental data after terminating

the Q-space at 10 $Å^{-1}$ and applying a spline through the data (FIG. S7 compares the raw and processed Q-space data). This processing (used to obtain Fig. 6 in the main text) was chosen to maximize the Q range while minimizing the ringing artifacts.

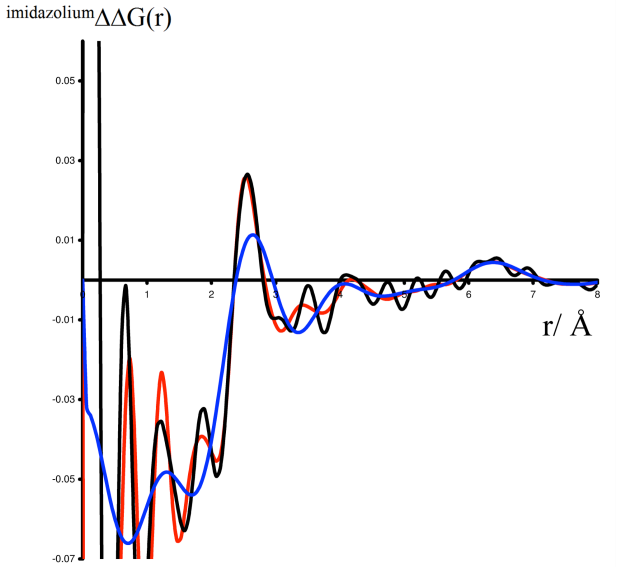


FIG. S6. Second order differences in the r-space *ΔΔG(r)* obtained by Fourier transforming the experimental Q-space data without any priori processing of the Q-space signal (black), with over-smoothing of the Q-space data leading to data loss and peak broadening (blue) and with a processing chosen to maximize the Q range while minimizing the ringing artifacts (red)

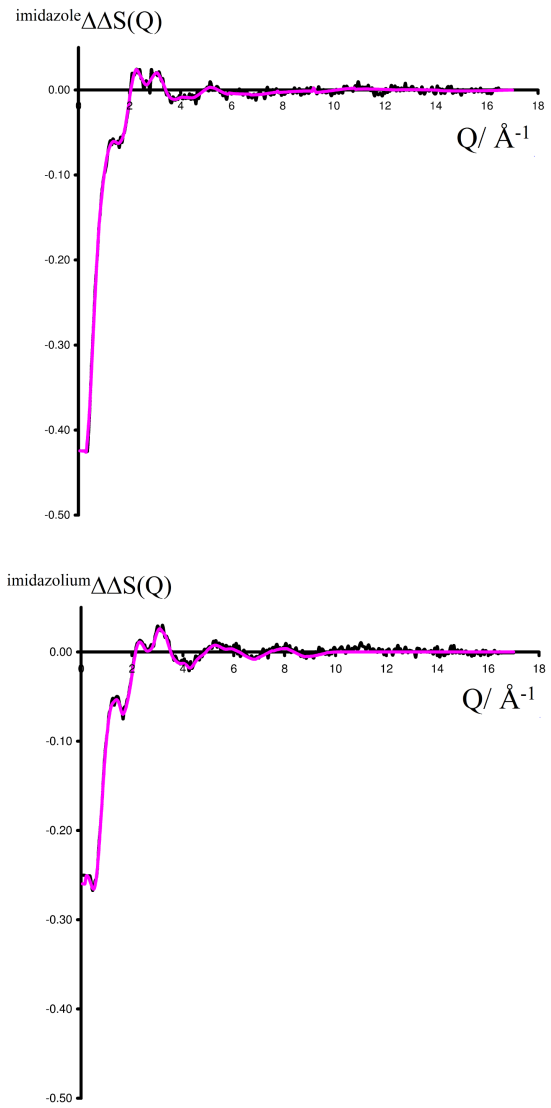


FIG. S7. Raw (black line) and processed (purple) second order differences ΔΔS(Q) for imidazole (top) and imidazolium chloride solutions (bottom).

## 7. Sensitivity of the neutron signal to the H-bonding geometry at N3

As discussed in the main text, the H-bonding geometry at N3 differs between force field and AIMD simulations: the received H-bond at N3 is more in the imidazole plane in the AIMD simulations. To explore how much the second order difference is sensitive to the H-bond geometry at N3, we perform a force field simulation where one water molecule H-bonded to N3 is constrained to stay in the imidazole plane. We compare the resulting computed second order difference $^{imidazole}\Delta\Delta G(r)$ to a simulation of the same system without any constraint on

the H-bond geometry (FIG. S**8**). In the unconstrained simulation, the H-bond is found markedly out of the imidazole plane (see main text). Both simulations were performed on a small system consisting of a single imidazole solute and 64 water molecules. FIG. S**8** clearly shows that the second order difference is rather insensitive to the H-bonded geometry at N3, so that neutron scattering alone cannot be used to further investigate this issue.

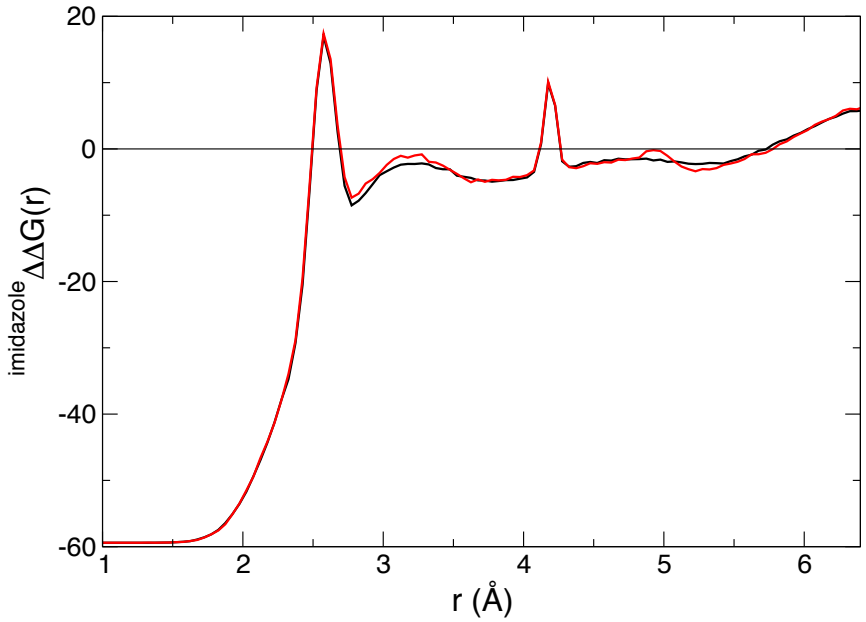


FIG. S8. Second order differences in the r-space *ΔΔG(r)* as obtained from MD simulations of a single imidazole in a box of 64 water molecules without constraints (black) and restraining one water donating a H-bond to N3 to stay in the imidazole plane (red).

## 8. Sensitivity of the neutron signal to the N3-Hw distance

To explore the sensitivity of the second order difference with respect to the H-bond length at N3, we replicate the simulation of the 3 m imidazole solution reducing the N3 van der waals radius σ, so that the N3-Hw average distance is reduced by 0.1 Å to match the AIMD simulations (see main text). FIG. S**9** compares the resulting second order differences in r space. Reducing the N3 van der waals radius results in a small shift to lower values of the peak just above 3 Å, which was assigned to correlations between *Hsub* and the hydrogen

donating a H-bond to N3. The feature above 4.5 Å is similarly shifted. Comparison with the experimental data in r-space is limited by the ringing of the Fourier transform, as already discussed, so that the change in the signal associated with a change in the N3-Hw distance is too small to draw any conclusions on this issue by comparison with neutron data.

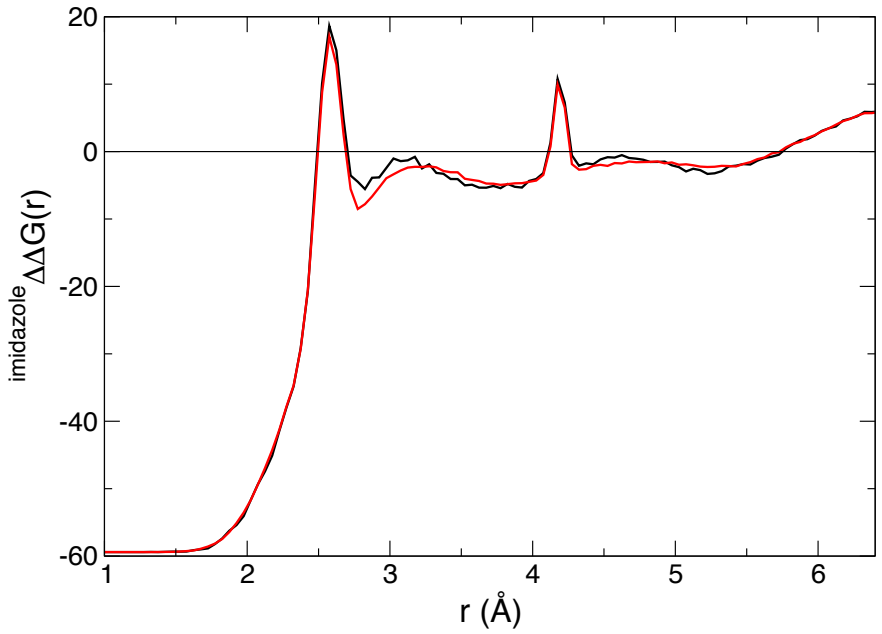


FIG. S9. Second order differences in the r-space *ΔΔG(r)* as obtained from MD simulations of a 3 m imidazole solution with CGenFF force field (black) and reducing the N3 van der waals radius so that the average N3-Hw distance is similar as in the AIMD simulation (red).